On the role of aerosols, humidity, and vertical wind shear in the transition of shallow to deep convection at the Green Ocean Amazon 2014/5 site

Sudip Chakraborty[1], Kathleen A. Schiro[1], Rong Fu[1], J. David Neelin[1]

1. Department of Atmospheric and Oceanic Sciences, University of California, Los Angeles, Los Angeles, California

Abstract

The preconditioning of the atmosphere for a shallow-to-deep convective transition during the dry-to-wet season transition period (August–November) is investigated using Department of Energy (DOE) Atmospheric Radiation Measurement (ARM) GoAmazon2014/5 campaign data from March 2014 to November 2015 in Manacapuru, Brazil. In comparison to conditions observed prior to shallow convection, anomalously high humidity in the free troposphere and boundary layer is observed prior to a shallow-to-deep convection transition. An entraining plume model, which captures this leading dependence on lower-tropospheric moisture, is employed to study indirect thermodynamic effects associated with vertical wind shear (VWS) and cloud condensation nuclei (CCN) concentration on pre-convective conditions. The shallow-to-deep convective transition primarily depends on humidity, especially that from the free troposphere, which tends to increase plume buoyancy. Conditions preceding deep convection are associated with high relative humidity, and low-to-moderate CCN concentration (less than the 67th percentile, 1274 cm^{-3}). VWS, on the other hand, shows little relation to moisture and plume buoyancy. Buoyancy estimates suggest that the latent heat release due to freezing is important to deep convective growth under all conditions analyzed, consistent with potential pathways for aerosols effects, even in presence of a strong entrainment. Shallow-only convective growth, on the other hand, shows an association with a strong (weak) low (deep) level VWS and with higher CCN concentration.

1. Introduction

Deep convection is the primary source of global precipitation over the tropics and mid-latitudes (Houze, 2004) and has a large influence on extreme rainfall events like flood and droughts (Houze et al., 2015). Deep convection is also associated with strong latent heat profiles of the atmosphere (Yin et al., 2014; Schumacher et al., 2004). Investigating the meteorological parameters and suitable environmental conditions favoring the formation and evolution of deep convection is thus of interest to more accurately predict rainfall in climate models.

Climate models often exhibit large uncertainties in rainfall variability and projection over the Amazon (Vera et al., 2006; Li et al., 2006), due in large part to the poor parameterization and an inability to simulate the formation of deep convective clouds and their evolution. Shallow and congestus convection transports moisture from the atmospheric boundary layer (BL) to the lower and middle troposphere, thus allowing for the development of deep convection (Zhuang et al., 2017; Del Genio and Wu, 2010; Jensen and Del Genio, 2006). However, many previous studies illustrate difficulties in representing the shallow-deep evolution in models (Del Genio and Wu, 2010; Waite and Khouider, 2010). Direct connections between the shallow-to-deep convection evolution and the ambient environment as well as land surface are neither fully understood nor adequately represented in climate models. There are a number of factors that can potentially dictate whether shallow convection will develop into deep, precipitating convection, such as free tropospheric moisture, vertical wind shear, cold pool formation, cloud-aerosol interactions, and the diurnal cycle.

Many studies have investigated the role of total precipitable water and moisture content of the boundary layer (BL) on the strength and evolution of deep convections both over tropical land and ocean sites (Schiro et al., 2016; Holloway and Neelin, 2009). In addition, there are ample studies that show that free tropospheric moistening is important for deep convective evolution (Waite and Khouider, 2010; Zhang and Klein, 2010; Kumar et al., 2013; Sherwood et al., 2004). Additionally, vertical wind shear (VWS) is known to influence deep convective clouds by influencing the slantwise ascent of the moisture (Moncrieff, 1978), separating the updraft and downdraft regions. In a recent study, it was shown that deep tropospheric VWS (DVWS) has a significant impact on the lifetime of mesoscale convective systems (Chakraborty et al., 2016) and can regulate the anvil's formation (Koren et al., 2010; Weisman and Rotunno, 2004; Petersen et al., 2006; Kilroy et al., 2014; Harrison, 1992) as well as the updraft speed of the parcels (Weisman and Rotunno, 2004). On the other hand, low level VWS (LVWS) can influence the rainfall and total condensation within developing convection (Weisman and Rotunno, 2004). However, it is still not clear how deep or lower tropospheric VWS affects updraft buoyancy. In addition, aerosols can delay the formation of precipitation size hydrometeors, invigorating strong convection, while suppressing shallower and weaker convection (Rosenfeld et al., 2008; Koren et al., 2008; Lin et al., 2006; Andreae et al., 2004). Low to moderate aerosols enhance convective strength and such an influence depends on humidity (Chakraborty et al., 2016). Furthermore, satellite data analyses have suggested that during the dry-to-wet transition season over the Amazon, biomass burning aerosols can increase warm clouds through their indirect effect under higher relative humidity (RH) and moderate aerosol loading, whereas under lower RH and heavy aerosol loading conditions, biomass burning aerosols tend to decrease clouds (e.g., Yu et al., 2006). Thus, it is

suggested that relatively small changes in the BL and in the free troposphere, due to changes of humidity, wind profile, and aerosols can trigger or suppress deep convection. However, we lack a clear understanding of the influence of these parameters on the deep convective evolution from shallow convection, primarily due to observational constraints.

A few recent studies have investigated deep convective evolution and buoyancy using ground-based measurements over the Amazonia (Zhuang et al., 2017; Schiro et al., 2016). Schiro et al. (2016) found that given sufficient mixing in the lower troposphere, column water vapor can be used as a proxy to understand the impact of free tropospheric humidity on plume buoyancy related to deep convective evolution. Sensitivity of buoyancy to other factors in the Amazon was also suggested, such as BL and microphysical processes, but the role of aerosols or VWS on deep convective evolution from shallow clouds was not analyzed. Another study by Zhuang et al. (2017) suggested that wind shear plays no significant role in convective evolution and that convective available potential energy is highest during the transition period. However, they did not assess indirect effects of vertical wind shear on the thermodynamic environment and updraft buoyancy. Additionally, these studies primarily focus on the wet season when RH is high, yet not explicitly on the transition season when RH is lower and aerosol concentration can be high. It is thus unclear whether other variables, such as VWS and aerosols, influence the transition to deep convection, either directly or by indirectly modifying the thermodynamic environment, or whether there may be factors such as air mass source that simultaneously affect VWS or aerosols and contributions by humidity to onset of deep convection. A key to answering these questions

might be found by analyzing the pre-convective environment. Here, we examine the association of these variables with estimates of plume buoyancy prior to the formation of deep convection.

The DOE Atmospheric Radiation Measurement (ARM) Mobile Facility in Manacapuru, Brazil, established as part of the Green Ocean Amazon campaign (GoAmazon2014/5) provides a suite of ground based measurements with high spatial and temporal resolution from January 2014 to December 2015. We analyze profiles of entraining plume buoyancies and assess how deep convection may be affected by humidity, VWS, and aerosol concentrations seasonally. Our main interest is to assess the effects of these variables on shallow to deep convection transition in the dry-to-wet transition season (August-November) in an effort to shed light on factors that control the increasing frequency of shallow to deep convection transition that drives the monsoon onset (Wright et al., 2017).

2. Data and methodology

A suite of ground based observations from the GOAmazon campaign in Manacapuru, Brazil are employed in this study to better understand the shallow-to-deep convective transition. The main site is located at 3°12’ S, 60°35’ W at 50m altitude above sea level. The data for this analysis spans from March 2014 to November 2015. Selection of this period was based on data availability.

2.1 Data

The primary instrument used to distinguish between shallow and deep convection by estimating cloud boundaries is a zenith pointing 95 GHz W-band radar, which works in both a co-polarization and cross-polarization mode. The reflectivity data (valid range between -90 to 50

dBZ) have temporal and vertical resolutions of one second and 30 meters, respectively, that is provided as a function of height and time in the units of dBZ with measurement accuracy of 0.5 dBZ. This dataset is available from February 2014 to November 2015. In addition to using the radar data to identify the cloud top, we have also used the Micropulse Lidar (MPL) to co-detect the convective tops. This is to reduce the uncertainty of the detection (as well as false detection) of the shallow and deep clouds due to the radar attenuation problem. The MPL is a ground-based optical remote sensing system that determines the top and base heights of clouds using a 30 second cloud mask based on the Z. Wang et al algorithm. Based on a time-resolved signal of transmitted and backscattered pulse, a real-time detection of the clouds can be made. These datasets are available from January 2014 to December 2015.

Vertical profiles of thermodynamic variables, such as zonal and meridional wind speed and direction, temperature, and relative humidity at pressure altitudes (from the surface to 3hPa) are derived from the balloon-borne sounding system These data are available from January 2014 to November 2015 and the measurements are taken daily at 0530, 1130, 1430 (occasional), 1730, and 2330 GMT. Radiosonde data provide information about meteorological and thermodynamic profiles, such as humidity, temperature, wind speed and direction.

Since we are also interested in understanding the role of aerosols on the convective transition, we have used datasets from the aerosol observing system (AOS) that provides in situ aerosol absorption and scattering coefficients as functions of the particle size and wavelength at the surface. The AOS also provides information about particle number concentration, size distribution, and the chemical composition of the particles, and has a cloud condensation nuclei

(CCN) particle counter that measures the CCN concentrations at a temporal resolution of one minute. It passes aerosol particles through thermodynamically unstable supersaturated water vapor in a column and the water vapor condenses on the aerosol particles. Particles that grow larger are counted. In this way, they measure the activated ambient aerosol particle number concentration that can be activated as CCN. We analyze CCN in this study to understand the influence of ambient aerosols on deep convection.

2.2 Methods

We calculate the mean buoyancy perturbation profiles between the environment and an entraining plume for ensembles of events in which shallow and deep convective characteristics are defined as described below. This permits investigation of the thermodynamic effect of BL humidity (between surface and 950 hPa), free tropospheric relative humidity (between 850 and 400 hPa), low level VWS, deep tropospheric VWS, and CCN concentrations. Low-level VWS is defined as the difference of the mean wind speed (zonal, since meridional wind difference is smaller) between the two 100 mb thick layers centering at 937 hPa and 737 hPa (Weisman and Rotunno, 2004); the deep level VWS is the difference between the layers centering at the 887 hPa and 287 hPa pressure levels (Chakraborty et al., 2016; Petersen et al., 2006). We calculate VWS by subtracting the mean wind speed of the top layer from that of the bottom layer.

We define shallow convection as having a cloud top height (CTH) below 4 km above the surface with a convective depth of more than 2 km. Deep convection is identified when CTH extends 8 km or more above the surface with a depth of more than 6 km (Wang and Sassen, 2007). In order to avoid errors related to the attenuated radar and Lidar pulses, we used both

146 the radar reflectivity (>-5 dBZ; Wang and Sassen 2007) and CTH derived from the MPL to identify
147 shallow and deep convection. From the radar dataset, we first separate the shallow convection
148 based on whether they remain shallow cloud until demise or whether they grow into deep
149 convection with time. Since we are interested in understanding why some shallow convection
150 evolves into deep convection while others do not, we investigate the meteorological,
151 thermodynamic, and aerosol properties before these shallow clouds form. Conditions before
152 shallow convection, which grows into deep convection with time, are considered to be "before
153 shallow-to-deep", or BSHDP. On the other hand, conditions pertaining to shallow convection
154 that stays shallow are considered to be "before-shallow" (BSH). For the information regarding
155 the profiles of RH, temperature, and wind speed during the BSH and BSHDP conditions, we use
156 the radiosonde measurements taken within two hours before the shallow or shallow-to-deep
157 convective event. CCN concentrations are averaged over ±30 minutes centered on the time of
158 radiosonde launch. These averaging time frames and radiosonde measurements are statistically
159 robust as shown in Schiro et al. (2016) where they show that temporal averaging up to and
160 including 3 hours yields robust statistics defining the transition to deep convection. In this study,
161 we show the impacts of CCNs based on 30 minutes average before and after the radiosonde
162 measurement. We estimate mixing ratio profiles for the BSH and BSHDP conditions from the
163 radiosonde data from a series of equations:

164 $$Vsat = 6.11 \times 10^{\frac{7.5 \times T}{237.3+T}} \quad (1)$$

165 $$mrsat = \frac{621.97 \times Vsat}{P - Vsa} \quad (2)$$

$$mr = mrsat \times RH \quad (3)$$

where Vsat is the saturation vapor pressure, P is the pressure, T is the temperature, RH is the relative humidity, and mrsat is the saturation mixing ratio (mr) at any level.

Lastly, we evaluate the variations of entraining plume buoyancies with RH, VWS, and CCN during BSHDP and BSH events to infer the influences of these environmental conditions on the development of deep convection. The methods described in Holloway and Neelin (2009) are used here to calculate the buoyancy profiles, defined as the virtual temperature (T_v) differences between the environment and an entraining parcel. Buoyancies are computed using mixing and micro-physical assumptions that span a range of possibilities. Results are presented primarily for Deep-Inflow-A (DIA) mixing with and without freezing. Deep-Inflow-B" (DIB) mixing with and without freezing, and a mixing assuming constant value of the entrainment parameter are presented in the SI to test sensitivity. Parcels originate from 1000 mb and T_v is interpolated in increments of 5 mb. The constant mixing case is an isobaric, fixed rate of linear mixing defined here to be 0.05 hPa^{-1}. DIA corresponds instead to an LES-based mixing scheme (Siebesma et al., 2007) in which the mixing coefficient depends inversely on height ($\alpha\ z^{-1}$), which has been shown to be a more realistic representation of buoyancy as compared to constant mixing (Schiro et al., 2016; Holloway and Neelin, 2009). In DIB deep-inflow mixing, mass flux increases linearly at low levels, but tapers in the mid-troposphere (Schiro et al., 2016; Holloway and Neelin, 2009). Schemes without freezing assume that the liquid water potential temperature is conserved while schemes that include freezing conserve the ice-liquid water potential temperature and all liquid is converted to ice when the plume reaches 0°C. *Schiro et al.* [2016] show results suggesting that

DIA might be a suitable scheme over the Amazon by illustrating the consistency between the sharp increase in precipitation observed with both increasing column water vapor (CWV) and plume buoyancies, and results are fairly similar between the two deep inflow schemes, so DIA is presented as representative.

3. Results

3.1. Mean characteristics of the BSH and BSHDP convective environments

To identify favorable atmospheric conditions before shallow and deep convective systems form, we evaluate differences in the mixing ratio averaged over all BSHDP (BSH) conditions relative to such averages over all the clear sky conditions, denoted mr', in all seasons (wet, dry, and dry-wet transition). Figure 1 shows that BSHDP conditions are associated with a higher mean mixing ratio throughout the troposphere than BSH conditions. During the transition season, such differences are the largest compared to the wet and dry seasons, especially above the 800 hPa level. Differences in mr' between the BSH and BSHDP conditions can reach up to 2 g/kg at the 600 hPa level during the transition period. Additionally, mr' during BSHDP conditions is deeper (up to 300 hPa) in the transition season as compared to the wet season (650 hPa) and dry season (500 hPa). Differences between mr' during BSH and BSHDP conditions are smaller during the wet season. This is likely due to the greater column moisture available throughout the wet season (Collow et al., 2016).

Similarly, we evaluate the mean RH associated with the BSH and BSHDP conditions at the 1000-850 hPa (lower troposphere), 850-700 hPa (lower free troposphere), 700-500 hPa (middle troposphere), and 500-350 hPa (upper-middle troposhere) levels during all three seasons. Figure

208 2 shows that the pre-shallow convective conditions are associated with smaller RH compared to
209 BSHDP conditions for all four layers during all three seasons; however, this difference is the
210 strongest and most significant during the transition period above 700 hPa.

211 Figure 3 shows the differences in mean wind speed before the BSHDP and BSH conditions.
212 BSHDP conditions are associated with a change in wind speed compared to the clear sky
213 condition up to a height of 300 hPa, whereas BSH conditions are associated with a stronger wind
214 up to an altitude of 750 hPa only. This suggests that shallow convection may occur in a low level
215 sheared environment in comparison to clear sky conditions.

216 Figure 4 shows that a higher CCN concentration is associated with BSH cases in
217 comparison to BSHDP cases in the transition season. It is unknown, however, whether such a
218 change of CCN concentration reflects aerosols' impacts on shallow to deep convection transitions
219 or merely an outcome of dry environments suppressing development of deep convection and or
220 the scavenging effect of rainfall in wet environment. The CCN levels associated with BSH are
221 comparable to those for clear sky or no-cloud (NC) cases, while those associated with BSHDP are
222 lower. For the local region of the data considered in classifying the events, the CCN observation
223 is prior to the convection, so local scavenging effects by wet deposition associated with
224 convection are excluded. However, we cannot exclude that convection-related scavenging may
225 have occurred upstream in the air mass prior to events, and that this could occur more frequently
226 under conditions that tend to lead to BSHDP events. During the dry and wet seasons, there are
227 no clear and significant difference in CCN concentration between the BSHDP and BSH conditions.

228 **3.2. Examining direct thermodynamic effects from humidity on buoyancy**

To examine the connection between humidity, vertical wind shear, and aerosols on the pre-conditioning of the convective environment and how they impact the conditional instability of the environment, we calculate buoyancies for plumes originating in the boundary layer using simple entraining plume models. We compute differences between a plume's virtual temperature (T_v) and the T_v of the environment (T_v') and conditionally average profiles associated with BSH and BSHDP conditions separately based on percentiles of humidity. This allows us to explore how the large free tropospheric moisture anomalies shown in Fig. 1 relate to the conditional instability of the environment and prove to be favorable for the development of deep convection, in contrast to the lower humidity observed for shallow convective cases.

Figure 5 shows that very humid free-tropospheric relative humidity (FTRH) conditions in the upper tercile are associated with comparatively larger buoyancies during both BSH and BSHDP conditions. Though we choose to only show results for one mixing assumption (Deep-Inflow-A; Holloway and Neelin (2009)), this holds true under a range of mixing assumptions (as shown in Fig. S1 of the Supplement). All BSHDP profiles are buoyant above 800 mb for any amount of free tropospheric humidity, which highlights the success of the deep-inflow scheme (with freezing) in capturing positive buoyancy for observed cases of deep convection. Profiles associated with higher humidity in the upper tercile (>66.67 ‰; >70%) have significantly larger buouyancy than other profiles. For BSH conditions (Fig. 5c), low (<33.33‰; <43%) and moderately (33.33-66.67‰; <51%) humid environments are suitable for shallow convective development only; however, as FTRH increases between 51% (66.67 ‰) and 71% (99.99 ‰), such profiles appear consistent with the formation of deep convective clouds — if the plume was able to reach to the freezing level and the release of latent heat were available for additional

buoyancy. The buoyancy profiles corresponding to instances of shallow-only convection have a deeper layer of negative buoyancy than BSHDP cases, on average. This may be one factor acting to suppress what may otherwise be an environment favorable for deep convection at high humidity.

An important conclusion is that without some occurrence of freezing, the possibility of a transition from shallow to deep convection is significantly reduced in all BSHDP cases (Betts, 1997). Here, all condensate is frozen when the parcel temperature drops below 0^{o}C, a useful limiting case that permits the impacts of freezing to be seen clearly. In practice, the freezing will occur over some layer, and will depend on nucleation processes (Rosenfeld et al., 2008). Though not explicitly tested in our analysis here, this also suggests that the effects of aerosols on freezing microphysics are likely to be impactful to the shallow-to-deep transition. There is some sensitivity to other entrainment schemes chosen; for instance, Deep-Inflow-B cases (Supporting Figure S1) show positive buoyancy profiles up to 200 hPa, yet the total buoyancy is smaller compared to that in the Deep-Inflow-A cases. These differences are attributed to the different mixing rates in the lower free troposphere.

We also conditionally average T_v' profiles by boundary layer relative humidity (BLRH) in Figure 6. BSHDP profiles are buoyant up to 200 hPa for all BLRH values, most probably owing to a higher RH (>72%) as compared to BSH profiles. This, again, highlights that the buoyancy computations are successful in producing positive buoyancy for observed cases of deep convection. As in the case of FTRH, moderate to high BLRH (>72%) is associated with larger buoyancy for BSHDP conditions (Figure 6a), BSHDP profiles are more buoyant than BSH profiles (Figure 6c), and consideration of freezing is a must for the deep convective evolution (Figure 6b).

On average, as seen in Figs. 1 and 2, the BL mixing ratio and BLRH (respectively) are higher for BSHDP conditions than BSH conditions, which is also reflected in the range of values defining the terciles in the table of Fig. 6. Though likely not the limiting factor in the transition to deep convection, given the range of values observed for both BSH and BSHDP cases, BLRH and buoyancy are intimately connected.

3.3. Examining indirect thermodynamic effects from shear and CCN on buoyancy

Previous studies have shown that the vertical wind shear and aerosols concentration can influence convective intensity and rainfall. For example, VWS influences the rainfall and total condensation within developing convection (Weisman and Rotunno, 2004), slantwise ascent of the parcel (Moncrieff, 1978), storm rotation, maintenance, vorticity, updraft speed (Weisman and Rotunno, 2000), and lifetime (Chakraborty et al., 2016). Though detailed microphysical properties are not considered in our simple plume calculations, it is worth noting that a recent study by (Wu et al., 2017) found that lower troposheric wind shear promotes the droplet collision and growth inside the shallow clouds by the production of turbulant kinetic energy. On the other hand, Weisman and Rotunno (2004) using a two-dimentional vorticity simulation model found that increasing vertical wind shear depth from surface - 3 km (low) to surface - 10 km (deep) decreases the overall condensation and rainfall output.

However, whether and how vertical wind shear and aerosol concentrations affect the thermodynamic environment and thus bouyancy is not well-known, especially during the preconditioning period before the clouds form. Hence, we examine potential indirect effects of

VWS and CCN concentration on the thermodynamics of the convective environment and thus plume bouyancy.

We look at the effect of controlling for DVWS on buoyancy profiles in Figure 7. The results show that no significant changes in BSHDP buoyancy profiles occur through the range of DVWS from low (3 m/s) to high (18 m/s) values (Figures 7a and 7b), which is true even for the full range of mixing assumptions tested (not shown). However, DVWS conditions do appear related to buoyancy among the shallow convective cases sampled. Figures 7c and 7d show that for BSH events, buoyancy is largest in a layer between roughly 500-850 mb when DVWS is low (<33.33‰; <3.2 m/s); as DVWS increases, buoyancy in the mid-troposphere decreases.

Recalling from Figure 3 that BSH conditions are associated with a change in wind speed up to 750 hPa only, we also analyze the influence of the lower tropospheric VWS (LVWS). As in the case of DVWS, controlling for changes in LVWS appears to have an insignificant influence on the BSHDP profiles (Figures 8a and 8b). However, unlike DVWS, strong LVWS (>66.67‰; >5.64 m/s) corresponds to increased buoyancy in the lower-troposphere, especially in the 500-850 mbar layer (Figures 8c and 8d). BSH conditions associated with weak to moderate LVWS (<5.64 m/s) are associated with significantly lower buoyancy. As a result, it can be inferred that a high LVWS or a low DVWS have associations with pre-theromodynamic conditions that might favor shallow convection.

The role of aerosols is interesting to parse, especially because of the higher amount of CCN concentrations associated with the BSH conditions. Figure 9 shows that low (0-33.33‰) to moderate (33.33-66.67‰) CCN concentrations are associated with increased buoyancy above

the freezing level for the BSHDP cases than in conditions of heavy CCNs (>66.67‰, Figure 9a). However, such an influence is not observed at altitudes below the freezing level and for BSH conditions (Figure 9c) or when we do not consider freezing in our buoyancy computations (Figures 9b and 9d). In Fig. 9a, the indirect effects of controlling for CCN on buoyancy above the freezing level are notable, with the thermodynamic conditions becoming less favorable for deep convection with increasing CCN. It is thus possible that higher CCN concentrations modify the thermodynamic environment such that they disfavor deep convective development, even among deep convective cases. The caveat should be noted that the results could instead imply an association of high CCN concentrations with other factors that modify the thermodynamic environment in this way. It is important to note that for roughly the same CCN concentrations in the middle tercile, the buoyancy profiles for BSH and BSHDP cases are starkly different above the freezing level. Therefore, though CCN are associated with modification of the thermodynamic environment, an effect on the buoyancy of convective plumes, this suggests that other more dominant variables provide leading controls on the transition to deep convection (e.g. humidity). It is thus of interest to consider covariability between humidity and the dynamical and microphysical variables analyzed.

In Figure 10 we calculate the conditional probability of occurrence of these conditions in the given bin (number of samples of BSHDP and SHDP (or BSH and SH) / total number of samples in a bin, in %) of both BSHDP and SHDP (during shallow-to-deep transitions) and BSH and SH (during shallow convection) conditions with respect to humidity and CCN concentrations. Values are shown only if the total number of samples in a bin is greater than 5. Figure 10a shows that BSHDP and SHDP conditions occur predominantly above 80% FTRH. However, BSH and SH

conditions (Figs. 10 b, d, and f) occur most frequently at lower values of FTRH with a peak probability of occurrences between 40-60% FTRH. Figure 10a shows that BSHDP and SHDP conditions occur at high FTRH and low-to-moderate (below the 67th percentile, i.e., 0-1200 cm^{-3}) values of CCN concentrations. High CCN concentrations (>1200 cm^{-3}) (Rosenfeld et al., 2008) and low RH (<60%) correspond to probabilities below 20%. For BSH and SH conditions (Figure 10b), such occurrences are associated with a relatively dry (40-70% FTRH) environment with optimal CCN concentrations ranging from 400-2000 cm^{-3}. This suggests that low to moderate concentrations of CCN and high humidity are associated with deep convection. This association is in part qualitatively consistent with the hypothesis that high CCN concentration can reduce the vigor of the convection by reducing the effect of convective available potential energy (*Rosenfeld et al.*, 2008). Quantitatively, it should be noted that the CCN values corresponding to strong precipitation are lower than the 1200 cm^{-3} optimum for Convective Available Potential Energy release illustrated in their buoyancy estimates. Figure 10 also has the strongest association of BSHDP and SHDP conditions with the lowest CCN concentrations, i.e. we do not detect a reduction at very low values with the data here. Low to moderate RH is not suitable for deep convective buoyancy, instead favoring shallow convective development (Figs. 1-2; Fig. 10 b, d, f). These results also suggest that CCN tend to have higher concentrations during BSH conditions. This is potentially due to the drier environment: High aerosol concentrations owing to drier conditions can form large numbers of small CCNs (Rosenfeld and Woodley, 2000) due to slower coagulation and coalescence; less wet deposition would also occur due smaller probability of precipitation. .

Consistent with the buoyancy profiles in Figs. 7 and 8, the conditional probability of occurrence of BSHDP and SHDP also shows that VWS does not have strong impact on the shallow to deep convective evolution (Fig. 10c, e). Again, our results suggest that higher FTRH is a primary control in the shallow-to-deep transition. On the other hand, shallow convection can occur for intermediate values of FTRH (40-70%). In such conditions, low values of DVWS (<8 m/s) and appreciable LVWS (4-12m/s) are associated with conditions favorable to the development of shallow clouds. This is consistent with increases in buoyancy observed in Figs. 7-8, though a range of conditions is depicted in Fig. 10 d and f.

We have also calculated the conditional probability of occurrences of the BSHDP as well as SHDP as well as BSHD(SH) conditions during the wet season to provide information on shallow-deep convective evolution during the wet season (Supporting Figure S2). In comparison, CCN concentrations are smaller during the wet season than the transition season, and it appears that humidity exerts the dominant control over CCN concentrations in the evolution from shallow to deep convection (Figs. S2a and b). We do not observe any increase in conditional probability of BSHDP events as CCN concentration increases during the wet season. BSHDP as well as SHDP events occur at higher relative humidity during the wet season (80%-100%, Figure S3 a, c, and e) than during the transition season (~80%, Figure 10 a, c, and e). Per the definitions of seasons adopted here, the sample size from the dry season (May-July) is too small to draw conclusions about the respective roles of CCN and VWS on the transition from shallow to deep convection.

4. Conclusion

This study employs a suite of ground-based measurements from the DOE ARM mobile facility in Manacapuru, BR as part of the GOAmazon campaign to investigate associations between meteorological parameters and CCN concentrations on an entraining plume's buoyancy before the formation of shallow or deep convective clouds during the transition season. We use cloud radar and micropulse lidar datasets to identify shallow convection and shallow-deep convection transitions. Radiosonde profiles measure wind speed and thermodynamic conditions up to two hours before shallow convection develops, and the aerosol observing system measures CCN number concentrations. Composites of CCN concentration, centered at the time of radiosonde launch, give some indication of the association between aerosols and other thermodynamic variables, and how these variables pre-condition the environment differently for shallow and deep convection.

Our results show that BSHDP conditions are associated with significantly higher mixing ratio perturbations and relative humidity above 800 hPa during the transition season compared to clear sky conditions. Such a humid free troposphere before the development of shallow-only clouds is not observed. Buoyancy increases as FTRH and BLRH increase for BSHDP conditions. BSH plumes are less buoyant than BSHDP parcels owing to the fact that they occur in less humid environments. Differences in the pre-convective humidity between the BSHDP and BSH conditions are largest during the transition season as compared to the dry and the wet seasons. These results suggest that moistening of the free troposphere is a necessary prerequisite for the development of deep convection.

Excluding the buoyancy effects of freezing above the 0°C isotherm, the buoyancy is insufficient for deep convective development, emphasizing the importance of freezing

400 microphysics on the shallow-to-deep convective transition. This confirms and quantifies the
401 potential for impacts on buoyancy by aerosol pathways operating via the freezing microphysics
402 (Rosenfeld et al., 2008) in presence of an important modification — the inclusion of sufficient
403 entrainment to give a realistic dependence on free tropospheric water vapor. Furthermore, it
404 confirms this potential in the range of thermodynamic environments relevant to the onset of
405 deep convection in the Amazon.

406 It is difficult to tease out a relation between dynamical and microphysical properties and
407 the conditional instability of the environment using plume buoyancies alone, but associations
408 can provide some indication of the favored environments for both shallow and deep convection.
409 Vertical wind shear does not appear to play a significant role in determining pre-thermodynamic
410 condition for the shallow to deep convective transition. However, a strong (weak) LVWS (DVWS)
411 appears to be related to the development of shallow convection that does not evolve to deep
412 convection. It is possible that this could be a causal influence of VWS, for example through the
413 entrainment process: if increased entrainment of dry air occurred due to a strong LVWS, it would
414 tend to limit the development of deep convection. However, it could simply be a noncausal
415 association of conditions leading to shallow convection with those leading to strong low-level
416 shear. Moreover, CCN might play a different role during the transition from congestus to deep
417 convective evolution as shown by Sheffield et al. (2015) using the Regional Atmospheric Modeling
418 System. Their study shows that congestus clouds in polluted conditions are associated with
419 greater ice mass and strong updraft speed, unlike the shallow to deep transition cases when CCN
420 concentrations in upper tercile reduce the convective buoyancy. It appears that condensate
421 reaching the freezing level is more important for congestus – deep convective evolution than the

422 association of the condensate loading effect for shallow-to-deep evolution. Congestus clouds
423 moisten the atmosphere, reach higher altitudes than shallow clouds, and often reach beyond the
424 freezing level to develop into deep convection. Thus, analyses of congestus-deep convective
425 transition using observational data sets are needed to understand how such evolution differs
426 from the shallow-to-deep convective evolution discussed here.

427 CCNs are thought to have complex interactions with deep convection, including through
428 their effects on delayed rainout of small drops, latent heating associated with freezing
429 microphysics, and droplet evaporation. In our analysis, the probability of deep convection is
430 greatest in association with low-to-moderate CCN concentrations (as defined through percentiles
431 for the observed conditions) and high relative humidity. This is qualitatively consistent with
432 previous findings that suggest that aerosol microphysical effects tending to invigorate deep
433 convective clouds saturate and reverse as CCN concentration increases beyond ~1200/cm^3
434 (Rosenfeld et al., 2008). Corresponding effects on cloud fraction have been suggested over the
435 Amazon (Koren et al., 2008) for aerosol optical depth about 0.25. Higher CCN concentrations
436 have been proposed to slow down the autoconversion process, on the one hand potentially
437 permitting more condensate to reach the freezing level, but on the other adding to condensate
438 loading with the maximum set by competing effects on the buoyancy for deep convection
439 (Rosenfeld et al., 2008). The condensate loading effect of higher concentrations of CCN might
440 inhibit the evolution of the shallow convections into deeper convection, reducing the possibility
441 of deep convective transition. Our analysis shows that a higher concentration of CCN in a dry
442 environment is associated with BSH conditions (Figure 4).

By these mechanisms, VWS and aerosols can potentially contribute to favorable (or unfavorable) conditions for deep convective evolutions. However, conditional instability for such developments primarily depends on humidity and the role of aerosols and VWS warrants further investigations. A caveat quantified here that does not seem to have been taken into account in other studies is that data stratified by conditions on aerosol or VWS concentrations can have substantial relationships with buoyancy that arise entirely from the thermodynamic environment. When making inferences about aerosol impacts using techniques that seek relationships between cloud or precipitation properties, we recommend controlling for or at minimum quantifying such covariability.

This study advances our capability to understand how some shallow convection evolves to deep convection and under what meteorological parameters and CCN concentrations such evolutions are favorable during the transition season over the Amazon. High FTRH and BLRH are required for a shallow-deep convective evolution during the transition season, which is associated with low-moderate concentrations of CCN. Deep convection appears unrelated to vertical wind shear in the transition season, whereas shallow convection has a weak association to strong LVWS and weak DVWS. It is worth nothing that the results of this study may differ across different regions. Use of different ACRIDICON-CHUVA datasets to test consistency with the southern Amazon, which is more prone to drought conditions, could prove to be a useful comparison.

ACKNOWLEDGEMENTS. This research was supported by the Office of Biological & Environmental Research within the Department of Energy (DOE), Office of Science, (DE-SC0011117 & DE-SC0011074). JDN and KAS were also supported under National Science Foundation Grant AGS-1505198 and National Oceanic and Atmospheric Administration Grant NA14OAR4310274. We acknowledge the providers of the DOE ARM datasets.

References

Atmospheric Radiation Measurement (ARM) Climate Research Facility. 2013(a), updated hourly. Meteorological Measurements associated with the Aerosol Observing System (AOSMET). 2014-03-02 to 2015-11-30, ARM Mobile Facility (MAO) Manacapuru, Amazonas, Brazil; MAOS (S1). Compiled by A. Koontz, J. Kyrouac and S. Springston. Atmospheric Radiation Measurement (ARM) Climate Research Facility Data Archive: Oak Ridge, Tennessee, USA. Data set accessed at http://dx.doi.org/10.5439/1025153.

Atmospheric Radiation Measurement (ARM) Climate Research Facility. 2013(b), updated hourly. Balloon-Borne Sounding System (SONDEWNPN). 2014-03-02 to 2015-11-30, ARM Mobile Facility (MAO) Manacapuru, Amazonas, Brazil; AMF1 (M1). Compiled by D. Holdridge, J. Kyrouac and R. Coulter. Atmospheric Radiation Measurement (ARM) Climate Research Facility Data Archive: Oak Ridge, Tennessee, USA. Data set accessed at http://dx.doi.org/10.5439/1021460.

Atmospheric Radiation Measurement (ARM) Climate Research Facility. 2014, updated hourly. W-Band (95 GHz) ARM Cloud Radar (WACR). 2014-03-02 to 2015-11-30, ARM Mobile Facility (MAO) Manacapuru, Amazonas, Brazil; AMF1 (M1). Compiled by A. Matthews, B. Isom, D. Nelson, I. Lindenmaier, J. Hardin, K. Johnson and N. Bharadwaj. Atmospheric Radiation Measurement (ARM) Climate Research Facility Data Archive: Oak Ridge, Tennessee, USA. Data set accessed 2017-08-08 at http://dx.doi.org/10.5439/1025317.

Atmospheric Radiation Measurement (ARM) Climate Research Facility. 2013, updated hourly. Cloud mask from Micropulse Lidar (30SMPLCMASK1ZWANG). 2013-03-02 to 2015-11-30, ARM Mobile Facility (MAO) Manacapuru, Amazonas, Brazil; AMF1 (M1). Compiled by C. Sivaraman and L. Riihimaki. Atmospheric Radiation Measurement (ARM) Climate Research Facility Data Archive: Oak Ridge, Tennessee, USA. Data set accessed 2017-08-08 at http://dx.doi.org/10.5439/1027736.

Andreae, M. O., Rosenfeld, D., Artaxo, P., Costa, A. A., Frank, G. P., Longo, K. M., and Silva-Dias, M. A. F.: Smoking rain clouds over the Amazon, Science, 303, 1337-1342, DOI 10.1126/science.1092779, 2004.
Betts, A. K.: The parameterization of deep convection., Nato Adv Sci I C-Mat, 505, 255-279, 1997.
Chakraborty, S., Fu, R., Massie, S. T., and Stephens, G.: Relative influence of meteorological conditions and aerosols on the lifetime of mesoscale convective systems, P Natl Acad Sci USA, 113, 7426-7431, 10.1073/pnas.1601935113, 2016.
Collow, A. B. M., Miller, M. A., and Trabachino, L. C.: Cloudiness over the Amazon rainforest: Meteorology and thermodynamics, J Geophys Res-Atmos, 121, 7990-8005, 10.1002/2016JD024848, 2016.
Del Genio, A. D., and Wu, J. B.: The Role of Entrainment in the Diurnal Cycle of Continental Convection, Journal of Climate, 23, 2722-2738, 10.1175/2009JCLI3340.1, 2010.
Harrison, S. J.: Fundamentals of Weather and Climate - Mcilveen,R, Scot Geogr Mag, 108, 133-133, 1992.
Holloway, C. E., and Neelin, J. D.: Moisture Vertical Structure, Column Water Vapor, and Tropical Deep Convection, Journal of the Atmospheric Sciences, 66, 1665-1683, 10.1175/2008JAS2806.1, 2009.

Houze, R. A.: Mesoscale convective systems, Rev Geophys, 42, Artn Rg4003

10.1029/2004rg000150, 2004.
Houze, R. A., Rasmussen, K. L., Zuluaga, M. D., and Brodzik, S. R.: The variable nature of convection in the tropics and subtropics: A legacy of 16years of the Tropical Rainfall Measuring Mission satellite, Rev Geophys, 53, 994-1021, 10.1002/2015rg000488, 2015.
Jensen, M. P., and Del Genio, A. D.: Factors limiting convective cloud-top height at the ARM Nauru Island climate research facility, Journal of Climate, 19, 2105-2117, Doi 10.1175/Jcli3722.1, 2006.
Kilroy, G., Smith, R. K., and Wissmeier, U.: Tropical convection: the effects of ambient vertical and horizontal vorticity, Q J Roy Meteor Soc, 140, 1756-1770, 10.1002/qj.2261, 2014.
Koren, I., Martins, J. V., Remer, L. A., and Afargan, H.: Smoke Invigoration Versus Inhibition of Clouds over the Amazon, Science, 321, 946-949, 10.1126/science.1159185, 2008.
Koren, I., Remer, L. A., Altaratz, O., Martins, J. V., and Davidi, A.: Aerosol-induced changes of convective cloud anvils produce strong climate warming, Atmos Chem Phys, 10, 5001-5010, 10.5194/acp-10-5001-2010, 2010.
Kumar, V. V., Jakob, C., Protat, A., May, P. T., and Davies, L.: The four cumulus cloud modes and their progression during rainfall events: A C-band polarimetric radar perspective, J Geophys Res-Atmos, 118, 8375-8389, 10.1002/jgrd.50640, 2013.
Li, W. H., Fu, R., and Dickinson, R. E.: Rainfall and its seasonality over the Amazon in the 21st century as assessed by the coupled models for the IPCC AR4, J Geophys Res-Atmos, 111, Artn D02111

10.1029/2005jd006355, 2006.
Lin, B., Wielicki, B. A., Minnis, P., Chambers, L., Xu, K.-M., Hu, Y., and Fan, A.: The Effect of Environmental Conditions on Tropical Deep Convective Systems Observed from the TRMM Satellite, Journal of Climate, 19, 5745-5761, 10.1175/jcli3940.1, 2006.
Moncrieff, M. W.: Dynamical Structure of 2-Dimensional Steady Convection in Constant Vertical Shear, Q J Roy Meteor Soc, 104, 543-567, 1978.
Petersen, W. A., Fu, R., Chen, M. X., and Blakeslee, R.: Intraseasonal forcing of convection and lightning activity in the southern Amazon as a function of cross-equatorial flow, Journal of Climate, 19, 3180-3196, Doi 10.1175/Jcli3788.1, 2006.
Rosenfeld, D., and Woodley, W. L.: Deep convective clouds with sustained supercooled liquid water down to-37.5 degrees C, Nature, 405, 440-442, Doi 10.1038/35013030, 2000.
Rosenfeld, D., Lohmann, U., Raga, G. B., O'Dowd, C. D., Kulmala, M., Fuzzi, S., Reissell, A., and Andreae, M. O.: Flood or drought: How do aerosols affect precipitation?, Science, 321, 1309-1313, DOI 10.1126/science.1160606, 2008.
Schiro, K. A., Neelin, J. D., Adams, D. K., and Lintner, B. R.: Deep Convection and Column Water Vapor over Tropical Land versus Tropical Ocean: A Comparison between the Amazon and the Tropical Western Pacific, Journal of the Atmospheric Sciences, 73, 4043-4063, 10.1175/Jas-D-16-0119.1, 2016.
Schumacher, C., Houze, R. A., and Kraucunas, I.: The tropical dynamical response to latent heating estimates derived from the TRMM precipitation radar, J Atmos Sci, 61, 1341-1358, Doi 10.1175/1520-0469(2004)061<1341:Ttdrtl>2.0.Co;2, 2004.
Sheffield, A. M., Saleeby, S. M., and van den Heever, S. C.: Aerosol-induced mechanisms for cumulus congestus growth, J Geophys Res-Atmos, 120, 8941-8952, 10.1002/2015jd023743, 2015.
Sherwood, S. C., Minnis, P., and McGill, M.: Deep convective cloud-top heights and their thermodynamic control during CRYSTAL-FACE, J Geophys Res-Atmos, 109, Artn D20119

10.1029/2004jd004811, 2004.
Siebesma, A. P., Soares, P. M. M., and Teixeira, J.: A combined eddy-diffusivity mass-flux approach for the convective boundary layer, Journal of the Atmospheric Sciences, 64, 1230-1248, 10.1175/Jas3888.1, 2007.
Vera, C., Silvestri, G., Liebmann, B., and Gonzalez, P.: Climate change scenarios for seasonal precipitation in South America from IPCC-AR4 models, Geophysical Research Letters, 33, Artn L13707

10.1029/2006gl025759, 2006.
Waite, M. L., and Khouider, B.: The Deepening of Tropical Convection by Congestus Preconditioning, Journal of the Atmospheric Sciences, 67, 2601-2615, 10.1175/2010JAS3357.1, 2010.

Wang, Z., and Sassen, K.: Level 2 Cloud Scenario Classification Product Process Description and Interface Control Document, Cloudsat Project, 5, 50, 2007.
Weisman, M. L., and Rotunno, R.: The use of vertical wind shear versus helicity in interpreting supercell dynamics, Journal of the Atmospheric Sciences, 57, 1452-1472, Doi 10.1175/1520-0469(2000)057<1452:Tuovws>2.0.Co;2, 2000.
Weisman, M. L., and Rotunno, R.: "A theory for strong long-lived squall lines" revisited, Journal of the Atmospheric Sciences, 61, 361-382, Doi 10.1175/1520-0469(2004)061<0361:Atfsls>2.0.Co;2, 2004.
Wright, J. S., Fu, R., Worden, J. R., Chakraborty, S., Clinton, N. E., Risi, C., Sun, Y., and Yin, L.: Rainforest-initiated wet season onset over the southern Amazon, Proceedings of the National Academy of Sciences, 10.1073/pnas.1621516114, 2017.
Wu, P., Dong, X. Q., Xi, B. K., Liu, Y. G., Thieman, M., and Minnis, P.: Effects of environment forcing on marine boundary layer cloud-drizzle processes, J Geophys Res-Atmos, 122, 4463-4478, 10.1002/2016jd026326, 2017.
Yin, L., Fu, R., Zhang, Y. F., Arias, P. A., Fernando, D. N., Li, W. H., Fernandes, K., and Bowerman, A. R.: What controls the interannual variation of the wet season onsets over the Amazon?, J Geophys Res-Atmos, 119, 2314-2328, 10.1002/2013jd021349, 2014.
Yu, H., Kaufman, Y. J., Chin, M., Feingold, G., Remer, L. A., Anderson, T. L., Balkanski, Y., Bellouin, N., Boucher, O., Christopher, S., DeCola, P., Kahn, R., Koch, D., Loeb, N., Reddy, M. S., Schulz, M., Takemura, T., and Zhou, M.: A review of measurement-based assessments of the aerosol direct radiative effect and forcing, Atmos. Chem. Phys., 6, 613-666, 10.5194/acp-6-613-2006, 2006.
Zhang, Y. Y., and Klein, S. A.: Mechanisms Affecting the Transition from Shallow to Deep Convection over Land: Inferences from Observations of the Diurnal Cycle Collected at the ARM Southern Great Plains Site, Journal of the Atmospheric Sciences, 67, 2943-2959, 10.1175/2010JAS3366.1, 2010.
Zhuang, Y. Z., Fu, R., Marengo, J. A., and Wang, H. Q.: Seasonal variation of shallow-to-deep convection transition and its link to the environmental conditions over the Central Amazon, J Geophys Res-Atmos, 122, 2649-2666, 10.1002/2016jd025993, 2017.

Figure Legends

Figure 1. Differences in the mixing ratio (mr') averaged over the before shallow (BSH) and before shallow-deep (BSHDP) conditions relative to that averaged over clear sky conditions during the a) wet, b) dry, and c) transition periods. Error bars show two-standard deviations of the data.

Figure 2. Mean RH of different levels during the BSH and BSHDP conditions. Error bars show two-standard errors of the data.

Figure 3. Differences in wind speed prior to BSHDP and BSH conditions during the transition period compared to the clear-sky condition. Solid lines represent the mean and the dotted lines represent the two-standard deviations of the wind speed for BSHDP and BSH cases.

Figure 4. Mean CCN concentrations (cm^{-3}) for the BSH, BSHDP, and clear-sky (NC) conditions over 30 minutes during all three seasons. Error bars show two-standard deviations of the data.

Figure 5. Profiles of delta Tv for BSH and BSHDP conditions under different cases of mixing and entrainment schemes compared to the mean environmental Tv condition obtained from the radiosonde data for different percentiles of free tropospheric RH (850-400 hPa) associated with the convections during the transition seasons. Shaded area represents two - standard errors for each profile. Values of corresponding FTRH are shown in the table. Total number of samples of BSHDP and BSH cases are 37 and 29, respectively. Solid (light blue shade), dotted (moderate blue shade), and dashed (dark blue shade) lines represent the conditionally averaged delta Tv values (two sigma error intervals) for the 0‰-33.33‰, 33.33‰-66.67‰, and 66.67‰-99.99‰ intervals, respectively.

Figure 6. Same as in Figure 5, but for different percentile values of BLRH. Values of corresponding BLRH are shown in the table.

Figure 7. Same as in Figure 5, but for different percentile values of deep tropospheric VWS. Values of corresponding DVWS are shown in the table.

Figure 8. Same as in Figure 5, but for different percentile values of lower tropospheric VWS. Values of corresponding LVWS are shown in the table.

Figure 9. Same as in Figure 5, but for different percentile values of CCN concentration. Values of corresponding CCN concentrations are shown in the table.

Figure 10. Contours of conditional probability (%) of (a, c, and e) BSHDP as well as SHDP; and (b, d, f) BSH as well as SH conditions with respect to (a), (b) FTRH and CCN concentrations, (c),(d) FTRH and DVWS, and (e),(f) FTRH and LVWS. Conditional probability of these conditions occurring in a given bin are estimated by dividing the number of samples of BSDHP and SHDP (or BSH and SH) conditions by the total number of samples in that bin. Blank areas correspond to bins for which neither shallow-deep nor shallow clouds are observed or total number of samples in that bin is less than 5. Total number of samples of BSHDP we well as SHDP, BSH as well as SH, and all the conditions (including clear sky) are 71, 49, and 565, respectively.

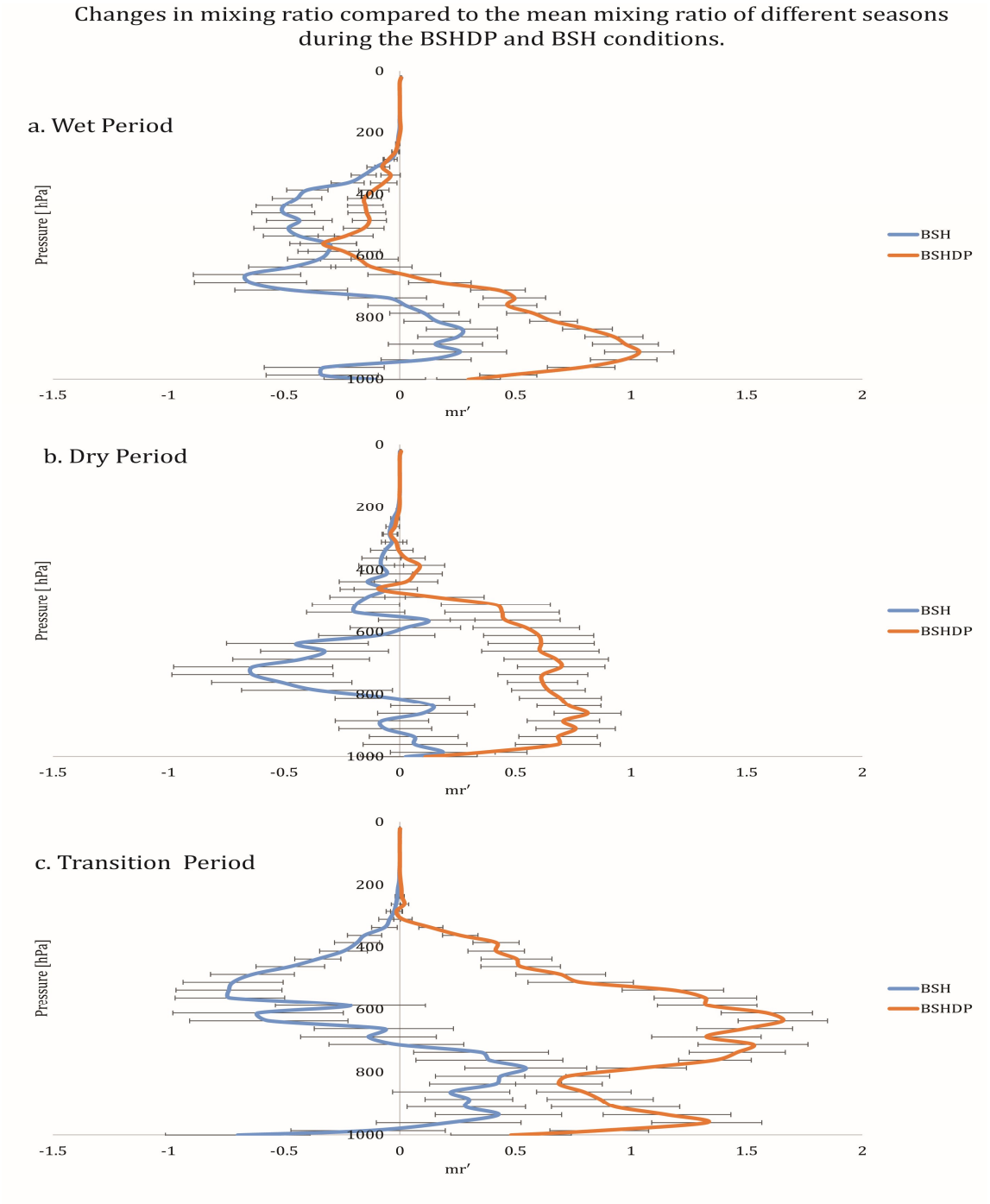
Changes in mixing ratio compared to the mean mixing ratio of different seasons during the BSHDP and BSH conditions.
a. Wet Period
b. Dry Period
c. Transition Period
Pressure [hPa]
mr'
BSH
BSHDP
0
200
400
600
800
1000
-1.5
-1
-0.5
0
0.5
1
1.5
2

Figure 1

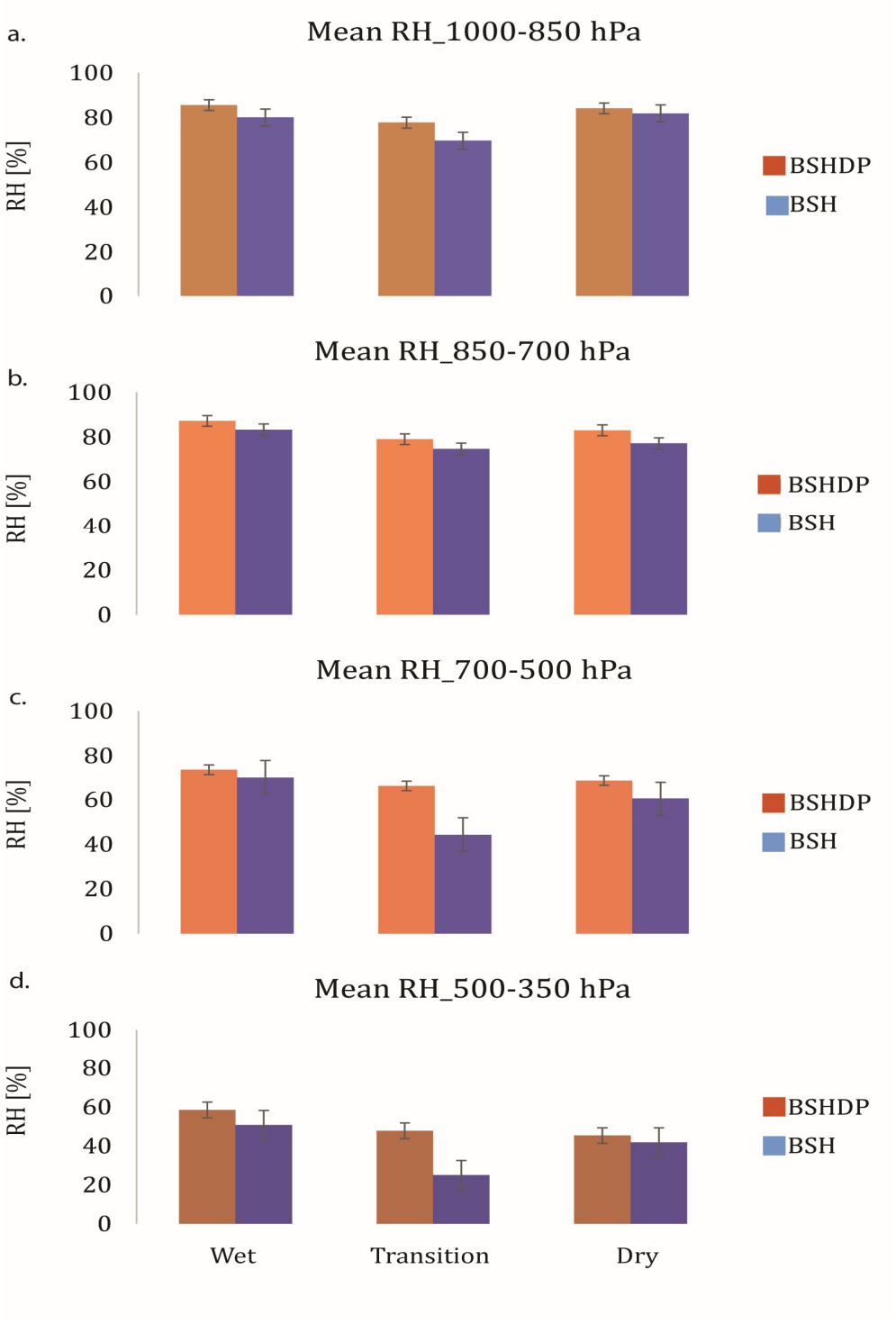
a.
Mean RH_1000-850 hPa
RH [%]
100
80
60
40
20
0
BSHDP
BSH
b.
Mean RH_850-700 hPa
RH [%]
100
80
60
40
20
0
BSHDP
BSH
c.
Mean RH_700-500 hPa
RH [%]
100
80
60
40
20
0
BSHDP
BSH
d.
Mean RH_500-350 hPa
RH [%]
100
80
60
40
20
0
BSHDP
BSH
Wet
Transition
Dry

Figure 2

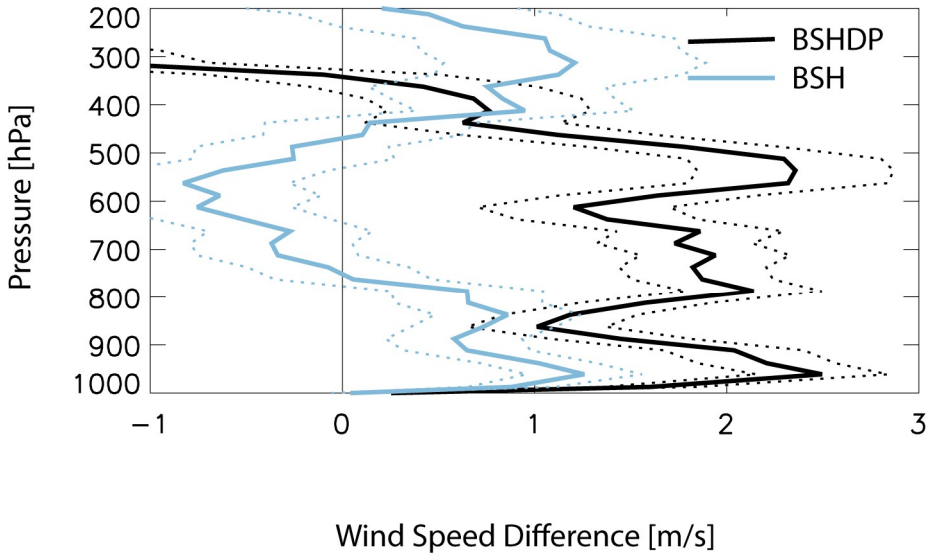
BSHDP
BSH
Pressure [hPa]
200
300
400
500
600
700
800
900
1000
−1
0
1
2
3
Wind Speed Difference [m/s]

Figure 3

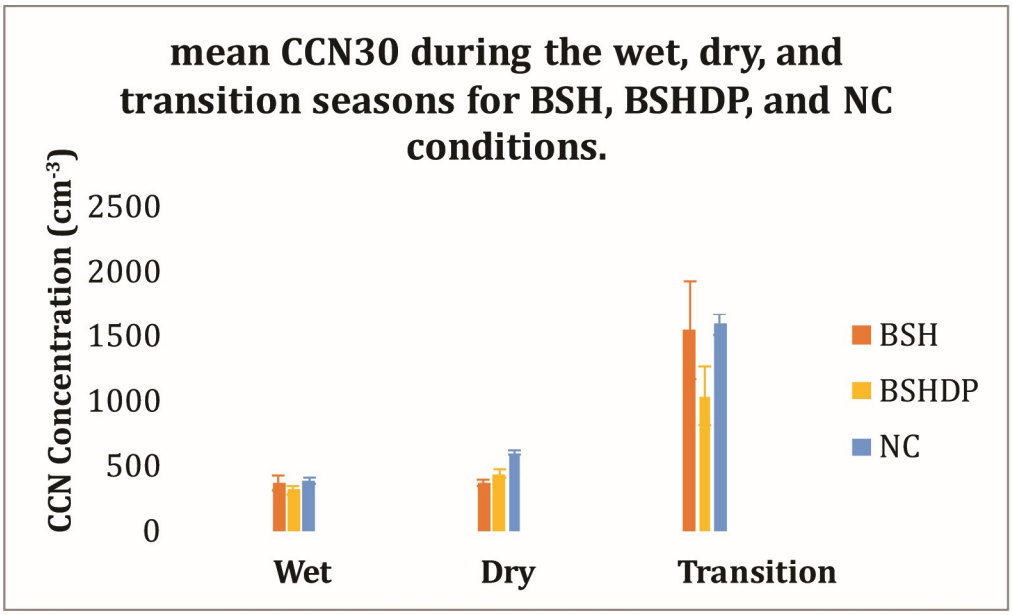
mean CCN30 during the wet, dry, and transition seasons for BSH, BSHDP, and NC conditions.
CCN Concentration (cm-3)
2500
2000
1500
1000
500
0
Wet
Dry
Transition
BSH
BSHDP
NC

Figure 4

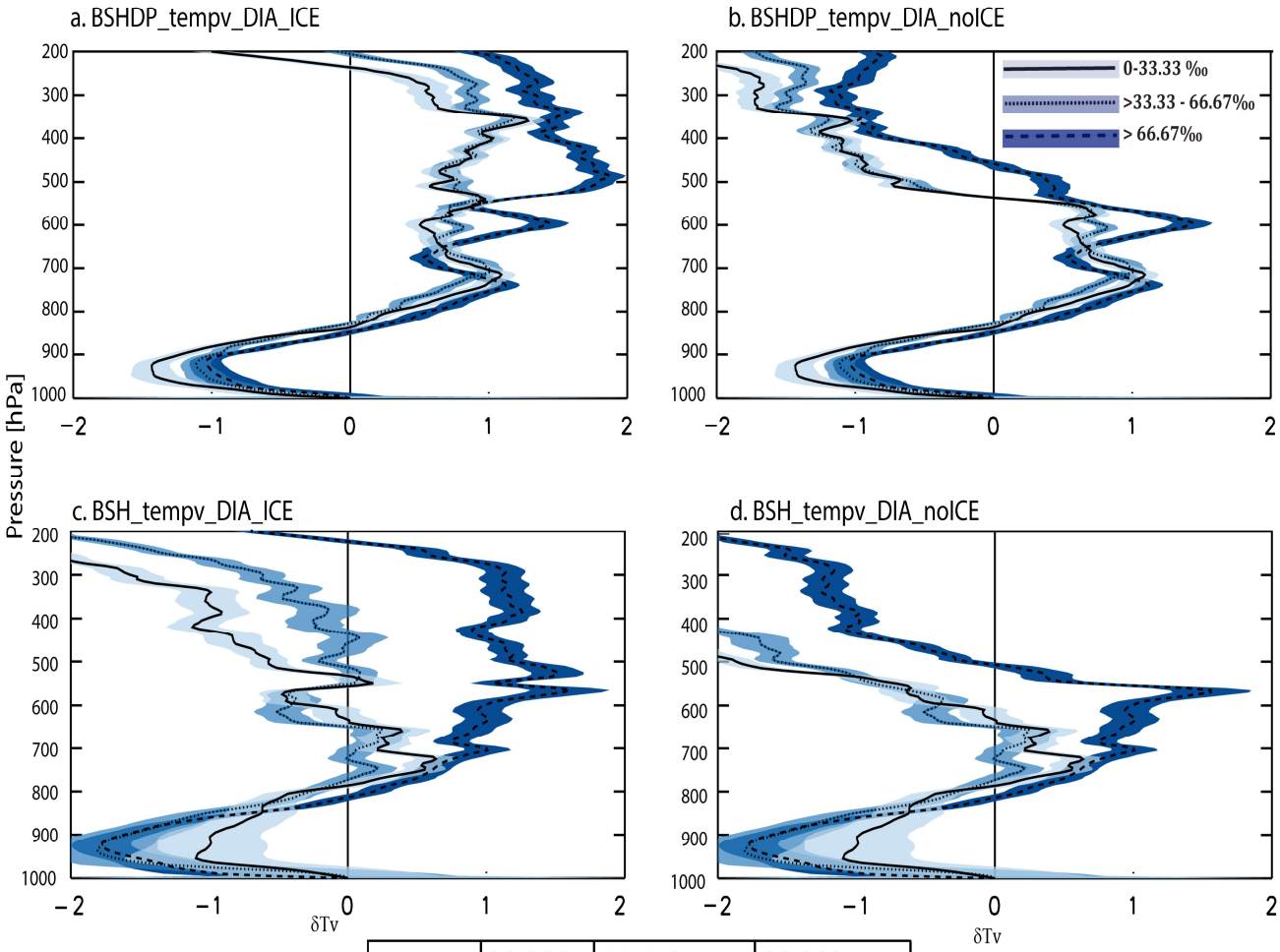

	33.33‰	66.67‰	99.99‰
BSH	43.31	50.99	70.65
BSHDP	63.37	68.24	84.71

Figure 5

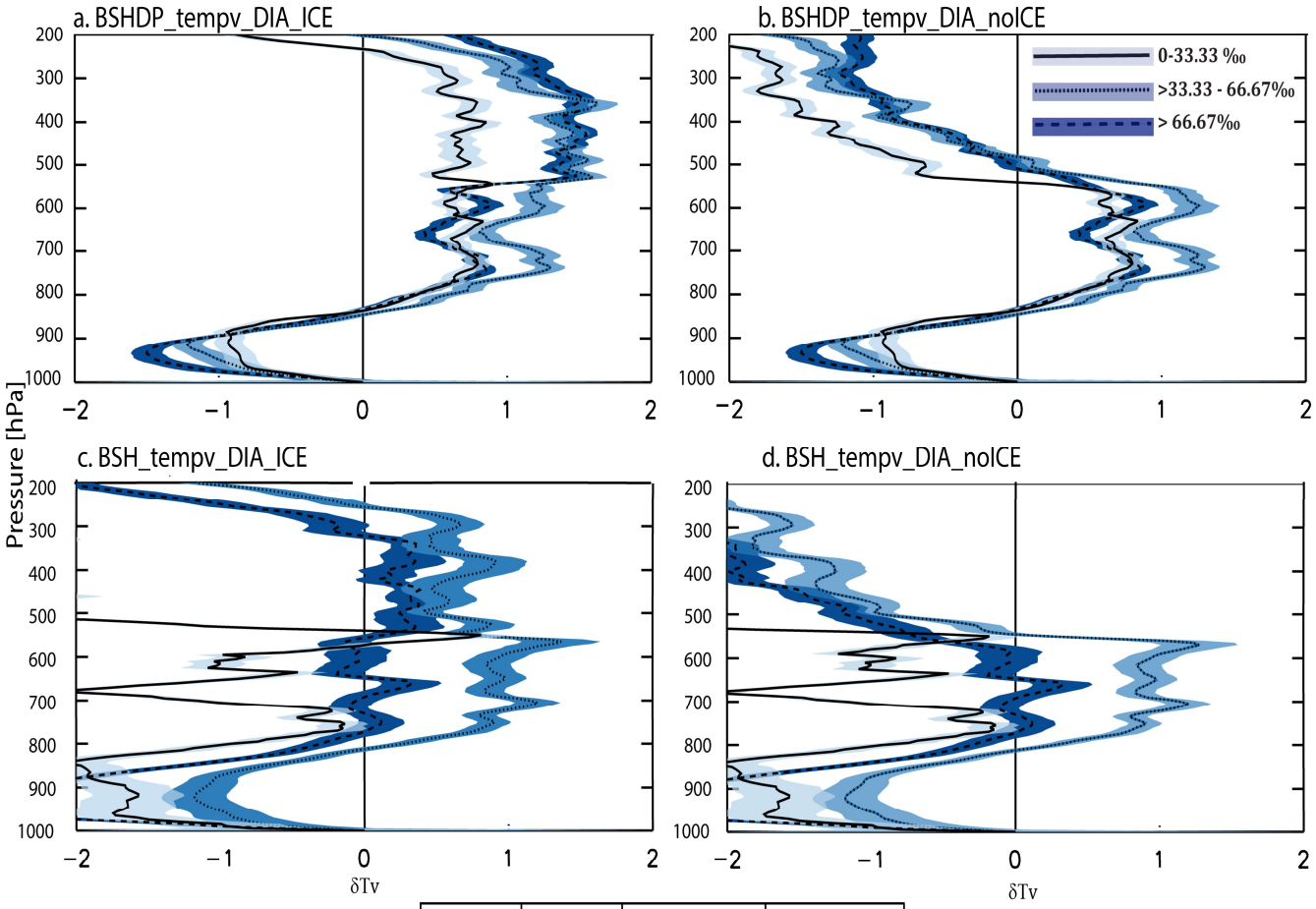

	33.33‰	66.67‰	99.99‰
BSH	57.11	72.5	91.76
BSHDP	71.99	76.36	92.89

Figure 6

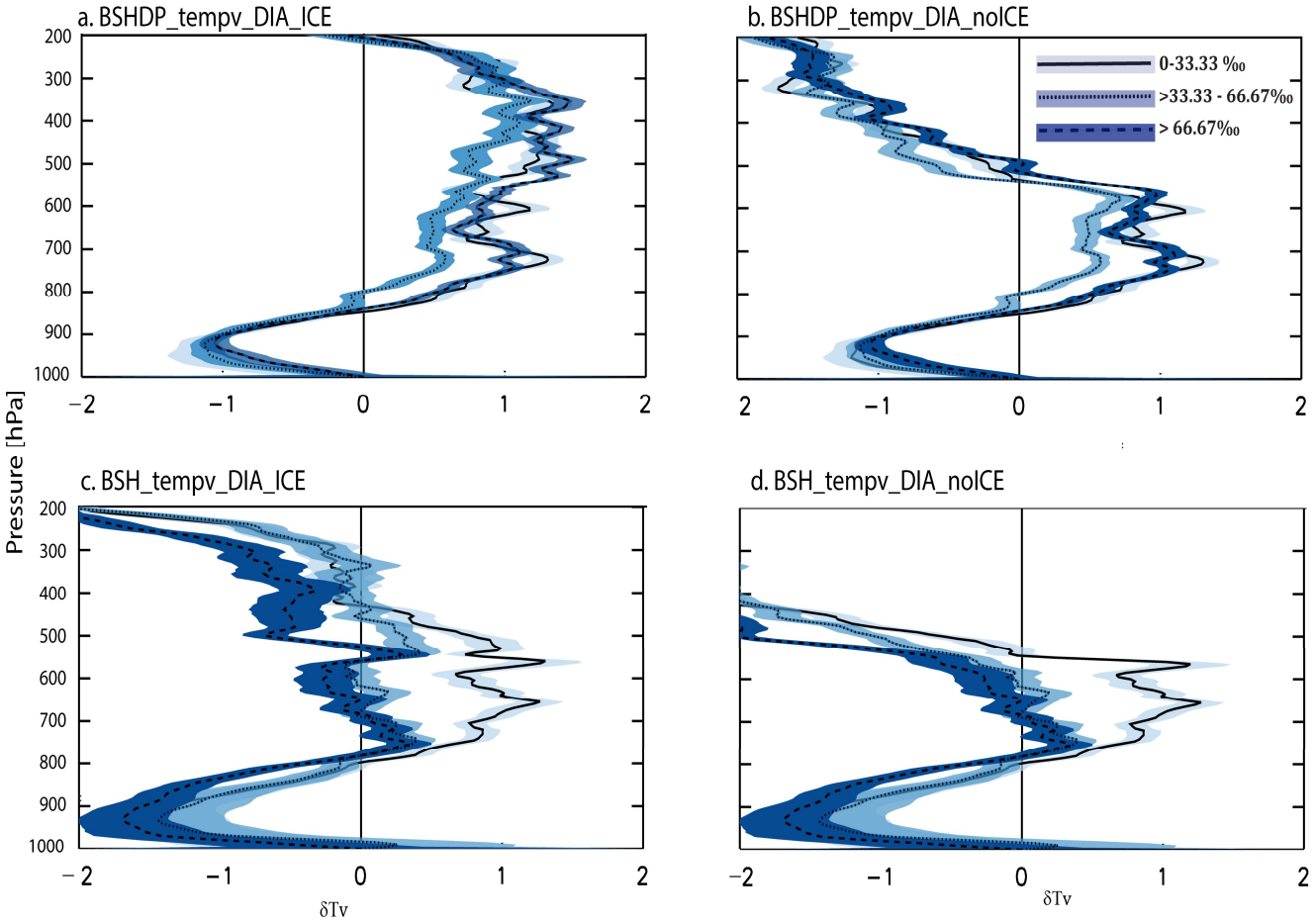

	33.33‰	66.67‰	99.99‰
BSH	3.2	9.25	17.62
BSHDP	3.38	7.04	18.39

Figure 7

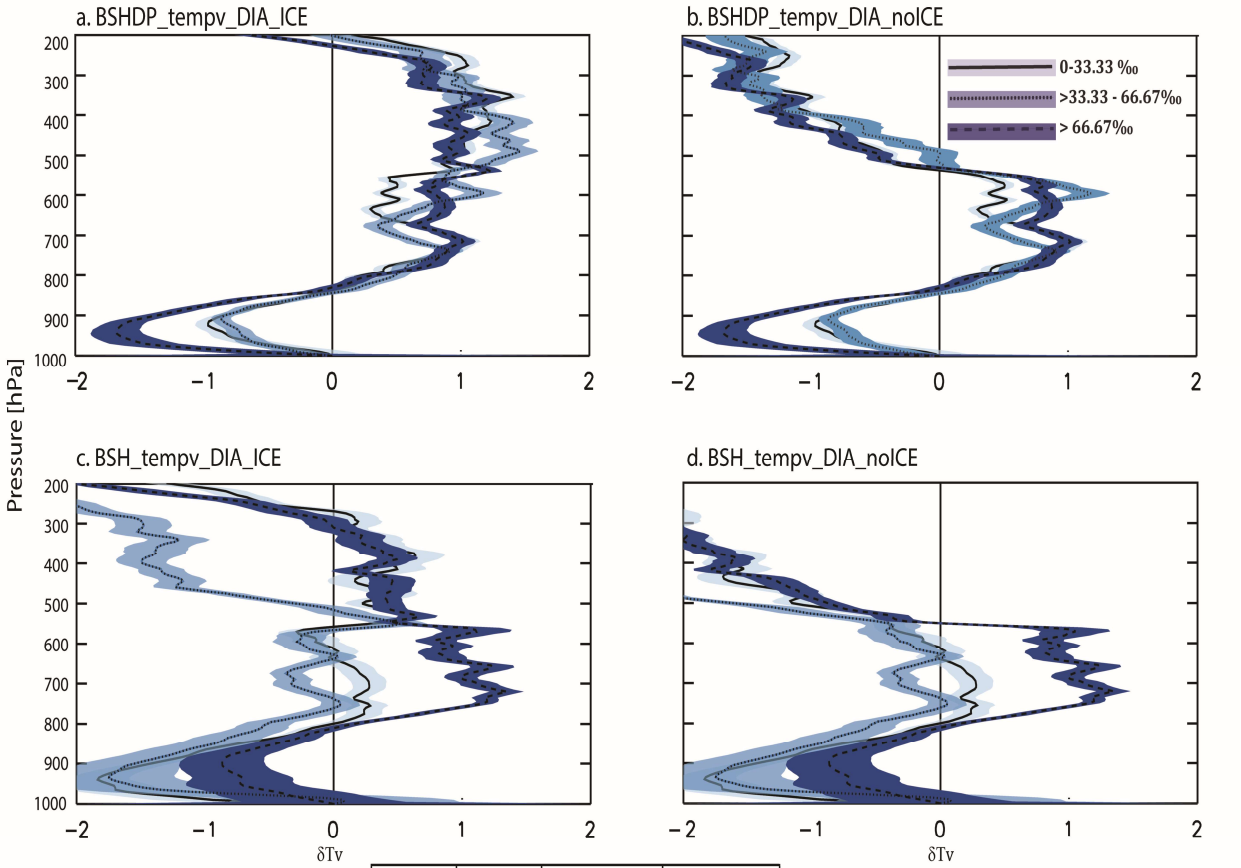

	33.33‰	66.67‰	99.99‰
BSH	3.87	5.64	9.52
BSHDP	2.69	4.3	12.81

Figure 8

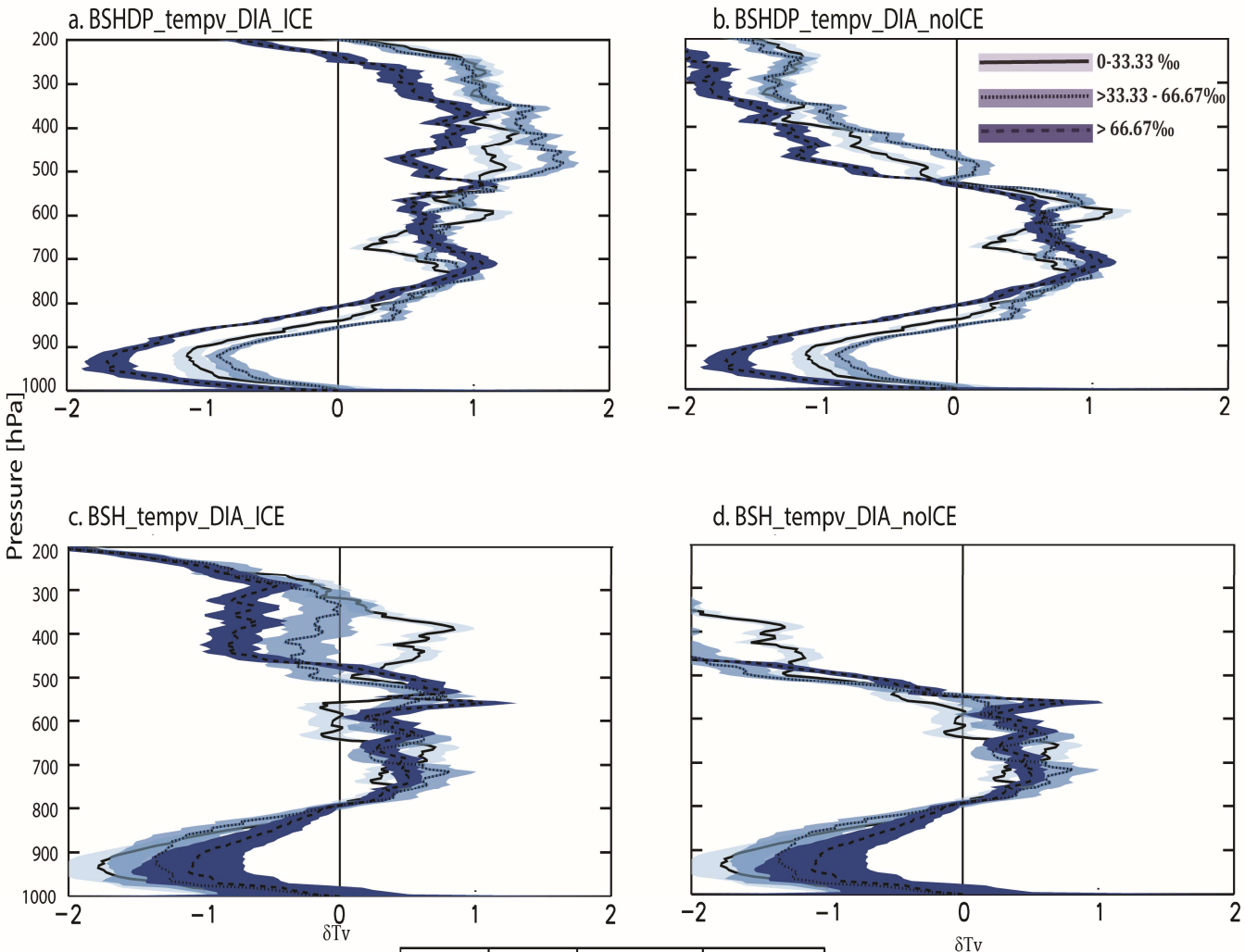

	33.33‰	66.67‰	99.99‰
BSH	735	1274	10422
BSHDP	565	912	7363

Figure 9

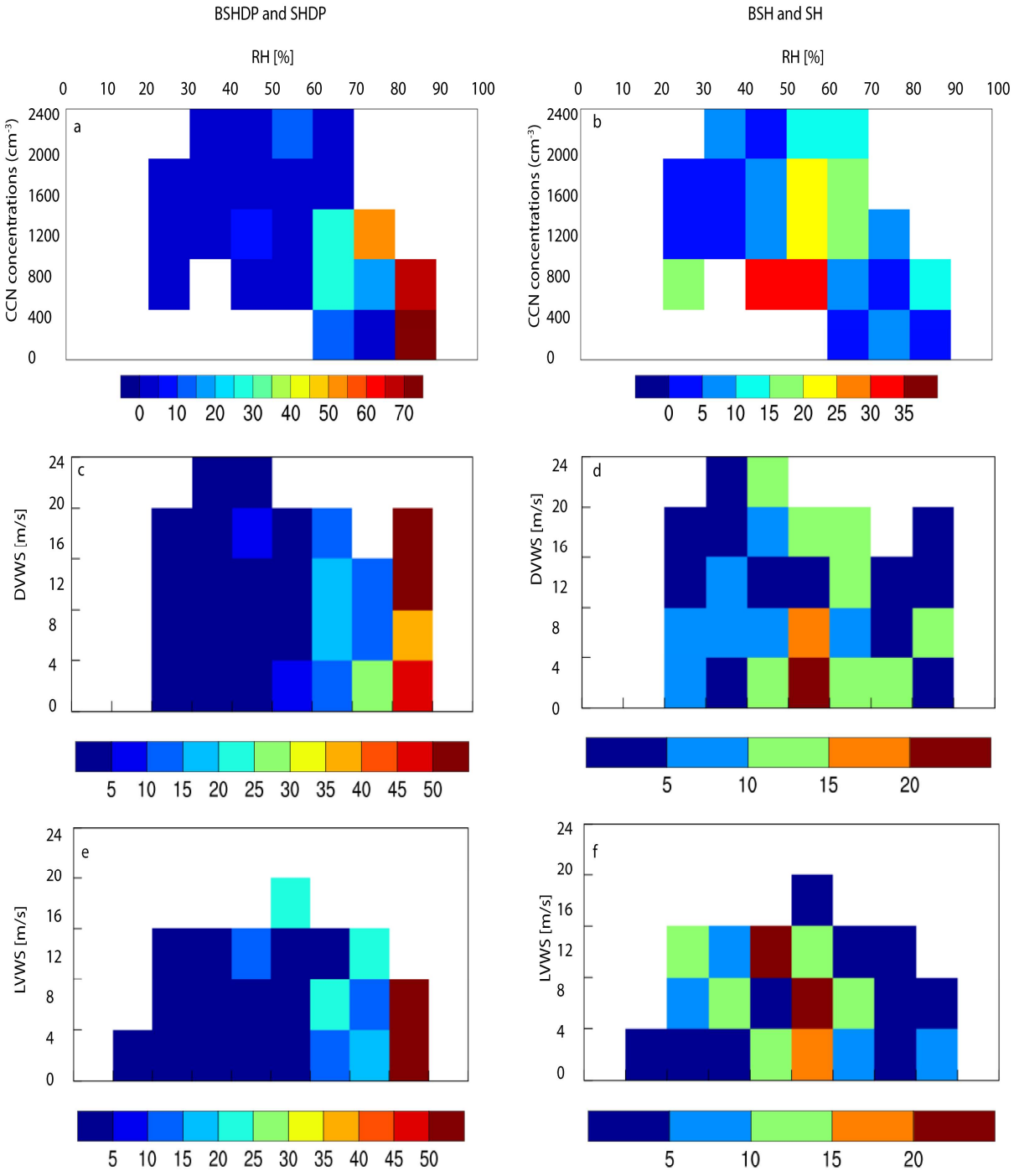
BSHDP and SHDP
BSH and SH
RH [%]
0 10 20 30 40 50 60 70 80 90 100
CCN concentrations (cm-3)
2400
2000
1600
1200
800
400
0
a
b
0 10 20 30 40 50 60 70
0 5 10 15 20 25 30 35
DVWS [m/s]
24
20
16
12
8
4
0
c
d
5 10 15 20 25 30 35 40 45 50
5 10 15 20
LVWS [m/s]
e
f

Figure 10